

1 **Multi-material direct ink writing (DIW) for complex 3D metallic structures**  
2 **with removable supports**

3  
4 *Chao Xu, Bronagh Quinn, Gilles L'Espérance, Louis Laberge Lebel, Daniel Therriault\**  
5  
6

7 Chao Xu, Bronagh Quinn, Prof. Louis Laberge Lebel, Prof. Daniel Therriault  
8 Mechanical engineering, Polytechnique Montreal  
9 C.P. 6079, succ. Centre-Ville, Montreal, QC H3C 3A7, Canada  
10 E-mail: Daniel.therriault@polymtl.ca  
11 Prof. L'Espérance  
12 Metallurgy engineering, Polytechnique Montreal  
13 C.P. 6079, succ. Centre-Ville, Montreal, QC H3C 3A7, Canada  
14

15 **Keywords:** additive manufacturing, direct ink writing, complex 3D metallic structures,  
16 removable support, multi-material  
17

18 **Abstract**

19 Direct ink writing (DIW) combined to post-deposition thermal treatments is a safe, cheap and  
20 accessible additive manufacturing (AM) method for the creation of metallic structures. Single  
21 material DIW enables the creation of complex metallic 3D structures featuring overhangs,  
22 lengthy bridges or enclosed hollows, but requires the printing supporting structures. However,  
23 the support printed from the same material becomes inseparable from the building structure  
24 after the thermal treatment. Here, a multi-material DIW method is developed to fabricate  
25 complex three-dimensional (3D) steel structures by creating a removable support printed from  
26 a lower melting temperature metal (i.e., copper) or a ceramic (i.e., alumina). The lower melting  
27 temperature metal completely infiltrates the porous steel structures for a hybrid configuration,  
28 while the ceramic offers a brittle support that can be easily removed. The influence of the  
29 support materials on the steel structure properties is investigated by the characterizing the  
30 dimensional shrinkage, surface roughness, filament porosity, electrical conductivity and tensile  
31 properties. The hybrid configuration (i.e., copper infiltrated steel structures) improves the  
32 electrical conductivity of the fabricated steel structure by 400% and the mechanical stiffness by

1 34%. The alumina support is physically and chemically stable during the thermal treatment,  
2 bringing no significant contamination to the steel structure.

3  
4

## 5 **Introduction**

6 Metallic structures fabricated through Additive manufacturing (AM), also referred to as three-  
7 dimensional (3D) printing, have been used as batteries,<sup>[1-2]</sup> medical implants,<sup>[3-4]</sup> and sensors<sup>[5-  
8 6]</sup> due to their key advantages, i.e., high mechanical and electrical properties, complex  
9 geometries, and mold-free manufacturing processes. The most established metal AM  
10 approaches are powder-bed based methods such as selective laser melting (SLM) and electron  
11 beam melting (EBM).<sup>[7-9]</sup> They use a laser beam or electron beam to locally fuse metallic  
12 particles in a powder bed to build a 3D object layer-by-layer. These methods feature short  
13 manufacturing time, high mechanical performance of the fabricated parts and very few  
14 restrictions on the printed geometry. However, they are limited by high cost, laser induced  
15 excessive oxidation, and residual stresses in the fabricated parts.<sup>[10-12]</sup>

16 Researchers developed many different metal AM methods to overcome the shortcomings of the  
17 powder-bed methods. Skylar-Scott *et al.* built metallic architectures from a water-based silver  
18 ink. The silver ink was extruded from a micro nozzle as a filament. The filament was sintered  
19 right after extrusion using a laser beam.<sup>[13]</sup> Freeform 3D metallic architectures featuring high  
20 resolution and high electrical conductivity were fabricated using this method. However, the  
21 laser beam sintering in the air would cause excessive oxidation and loss of alloying elements.  
22 Wang *et al.* developed an initiator-integrated 3D printing method to build metallic structures.<sup>[14]</sup>  
23 First, a polymer template of the 3D structure was built. Then metallic particles were deposited  
24 on the surface of the polymer template through electroless plating. Finally, the polymer  
25 template was etched away to achieve ultralight cellular metallic structures. This method enables  
26 the fabrication of complex 3D metallic structures featuring low density. However, the metallic

1 architecture is hollow and relatively thin after the polymer template is etched away, which leads  
2 to poor mechanical performances.

3 Direct ink writing (DIW) is an AM method, which usually relies on the extrusion of polymer  
4 solution (or melt), known as ink, through a micro-nozzle and the deposition of the extruded ink  
5 on a substrate layer by layer to create a 3D object.<sup>[15-16]</sup> Researchers adapted it to metal AM by  
6 printing from metallic inks.<sup>[17-20]</sup> The metallic inks are prepared by adding metal micro- or nano-  
7 particles to the polymer solution (or melt), which are used in DIW to build a metal-polymer  
8 composite 3D structure. To achieve a metallic structure featuring high mechanical and electrical  
9 performances, a post-deposition thermal treatment is performed to pyrolyze the polymer and to  
10 sinter the metal particles.

11 DIW of polymer can create complex 3D structures with large overhangs or lengthy bridges by  
12 printing support underneath them to hold the structures. Once the printing is completed, the  
13 sacrificial support is removed.<sup>[21-22]</sup> However, the utilization of a support does not work for  
14 DIW of metal, where a post-deposition thermal treatment is performed. If the support is  
15 removed before the thermal treatment at a moment when the polymer binder is pyrolyzed before  
16 the sintering of the metallic particles, the overhang features will collapse. Whereas, if the  
17 support printed from the same material is not removed before the thermal treatment, the support  
18 and the building structure will fuse together and become inseparable after the thermal treatment.  
19 Thus, the existed DIW methods are unable to fabricated complex 3D metallic structures  
20 featuring overhangs, length bridges or enclosed hollows.

21 Here, we propose a multi-material DIW method to fabricate complex 3D metallic structures  
22 with removable supports. This method consists of two steps: (a) room-temperature DIW of  
23 metal-polymer composite structures with metal- (or ceramic-) polymer composites supports,  
24 and (b) a post-deposition thermal treatment turning the as-printed metal-polymer composite  
25 structures to metal structures. **Figure 1a** shows a schematic of the multi-material DIW system  
26 and as-printed hollow sphere structures. The multi-material DIW system includes three major

1 components: (i) a computer controlled 3-axis robot, (ii) a pressure dispenser, and (iii) multiple  
2 ink syringes containing steel, copper and alumina inks. The inks are concentrated steel, copper  
3 and alumina microparticle suspensions dispersed in a polymer solution (i.e., polylactic acid /  
4 dichloromethane, referred to as PLA/DCM), respectively. The scanning electron microscope  
5 (SEM) images of the microparticles are shown in **Figure S1**. To fabricate a 3D metallic  
6 structure, e.g., a hollow sphere as shown in **Figure 1a**, supports are generated inside the hollow  
7 sphere to support the top overhang part and underneath the sphere to create a flat bottom which  
8 is compatible with the geometry of the substrate. Here, as a proof of concept, the supports are  
9 built using a secondary material (i.e., copper or alumina ink), while the building structure is  
10 printed with the primary material (i.e., steel ink). The steel-PLA composite structure with  
11 copper-PLA composite support is referred to as as-printed S-Cu, while the one with alumina-  
12 PLA composite support is referred to as as-printed S-Al<sub>2</sub>O<sub>3</sub>. These two types of supports are  
13 differently removed through the post-deposition thermal treatment. The lower melting  
14 temperature metallic support (i.e., copper) could be completely melted and infiltrated into the  
15 pores within the filament of the sintered structure to achieve a hybrid configuration. The  
16 ceramic support (i.e., ceramic) survives the temperature cycle without any significant sintering  
17 and can be easily removed without affecting the metallic structure.

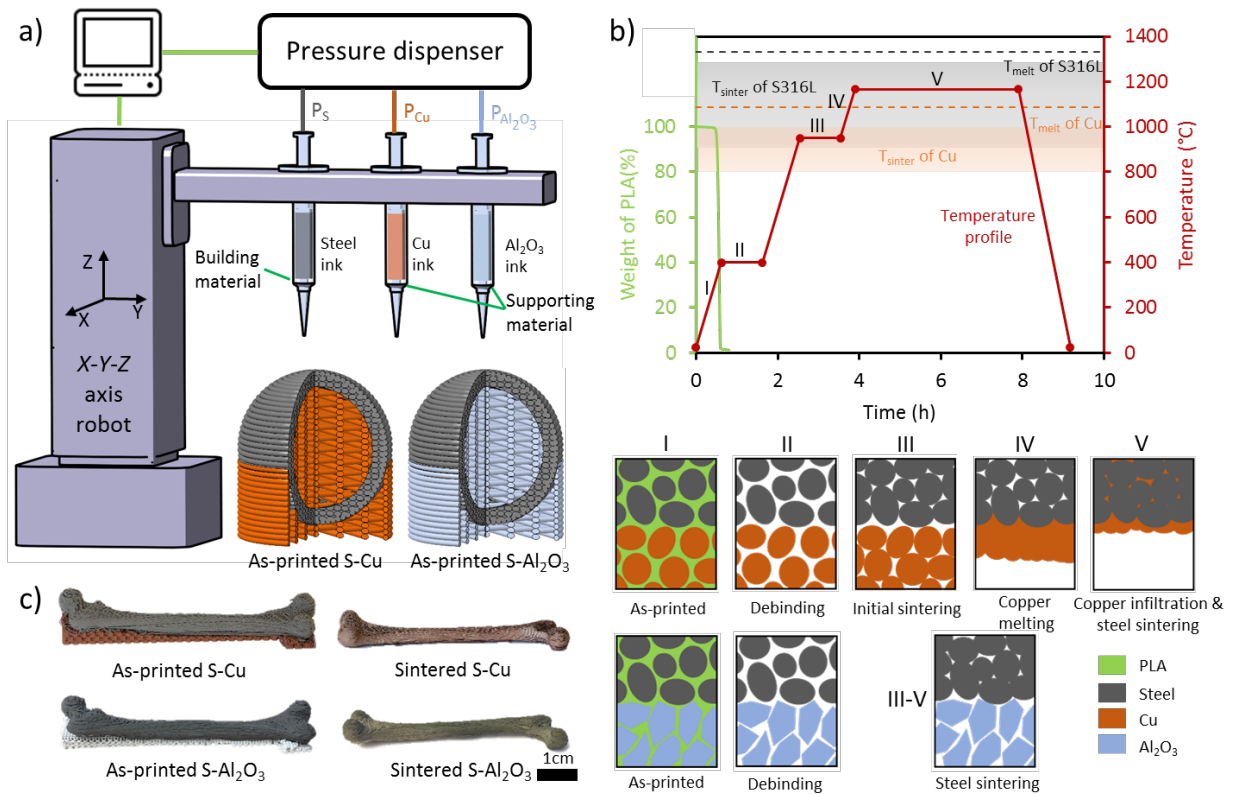
18 **Figure 1b** presents the temperature profile of the thermal treatment, the thermal gravity analysis  
19 (TGA) result of the polymer binder PLA under this temperature profile, the sintering  
20 temperature range and melting temperature of stainless steel 316L and copper.<sup>[23-24]</sup> In addition,  
21 a schematic is shown in **Figure 1b** illustrating the microstructure variations of the two-phase  
22 interface in the as-printed structures at five different stages during the thermal treatment. For  
23 S-Cu structures, Stage I is an as-printed structure at room temperature, where the steel and  
24 copper particles are bound by the PLA binder, respectively. Stage II consists of a one-hour  
25 plateau at 400°C for debinding. PLA binder is completely pyrolyzed as shown in the TGA curve,  
26 where the weight of the PLA binder rapidly drops within 7 min. The structure is held by the

1 friction forces among the steel particles and among copper particles, respectively. The  
2 temperature then is increased to reach a temperature plateau at 950°C for one hour (Stage III).  
3 This plateau temperature is selected to be in the sintering temperature range of S316L and  
4 copper, but is lower than their melting temperatures. The S-Cu structure is mechanically  
5 enhanced by initial sintering, where the necks appear among steel particles and among copper  
6 particles, respectively. After this stage, even if the support is removed, the bonding between the  
7 steel particles is strong enough to hold the building structure. During Stage IV, the temperature  
8 increases from 950°C to 1165°C, surpassing the melting temperature of copper (i.e. 1085°C).  
9 The copper support starts melting, while the steel structure is held in its original geometry by  
10 the sintering bonds generated during Stage III. Stage V is a four-hour plateau at 1165°C, where  
11 the steel particles are further sintered and the melted copper completely infiltrates the pores of  
12 the sintered steel structure by capillary forces. After this temperature profile, the as-printed S-  
13 Cu is turned into a steel structure infiltrated by the copper.

14 For S-Al<sub>2</sub>O<sub>3</sub> structures, Stages I and II are the as-printed structure at room temperature and the  
15 debinding process respectively, like those of the S-Cu structures. Since both the melting  
16 temperature of alumina (2040°C) and the lower limit of alumina sintering temperature  
17 (1800°C)<sup>[25]</sup> are much higher than the maximum imposed temperature (1165°C), the alumina  
18 particles are neither melted nor sintered, but remain as individual particles during the whole  
19 thermal treatment. Therefore, in Stages III to V, the alumina support preserves its shape mostly  
20 due to the friction forces among the alumina particles. The steel particles are sintered and form  
21 a strong steel keeping the original geometry. As the alumina support is weakly held by the  
22 friction forces, it does not fuse with the building structure and can be easily removed by hand  
23 after the thermal treatment.

24 **Figure 1c** shows the as-printed and sintered S-Cu and S-Al<sub>2</sub>O<sub>3</sub> printed using this method as a  
25 structure shaped as a human thigh bones at a scale of 1:7. The steel bone structure is 50% of

1 volume filled, while the support structure is 30% of volume filled. The supports provide a flat  
 2 bottom and hold up the overhang features for the bone to facilitate the printing on a flat substrate.  
 3 After the thermal treatment, the copper support melts and infiltrates into the sintered steel  
 4 structure, while the alumina support is removed easily by hand. Both sintered structures  
 5 preserve the original geometry of the human thigh bone with a uniform linear dimensional  
 6 shrinkage of 11%. To demonstrate the ability to build complex 3D metallic structure featuring  
 7 overhangs, an inverted “L” shape structure featuring a large overhang part is fabricated through  
 8 this method with a cubic support structure printed from a secondary material (**Figure S2**).



9  
 10 **Figure 1.** Multi-material DIW for complex 3D metallic structures with removable supports  
 11 consists of two steps: (a) room-temperature DIW of metal-polymer composite structures with  
 12 metal- (or ceramic-) polymer composites supports, and (b) a post-deposition thermal treatment  
 13 turning the as-printed metal-polymer composites structures to metal structures, and a schematic  
 14 shows the two-phase interface microstructures variations of the as-printed structures at five

1 different stages during the thermal treatment. (c) Optical images of as-printed and sintered S-  
2 Cu and S-Al<sub>2</sub>O<sub>3</sub> structures printed as a human thigh bones at a scale of 1:7.

3

#### 4 **Experimental Section**

5

6 *Ink preparation:* The steel particles are stainless steel 316L with a spherical shape and a  
7 diameter less than 20µm. The copper particles are spherical and less than 20µm in diameter.  
8 The steel and copper particles are purchased from US Research Nanomaterials, Inc. The  
9 alumina particles are irregular in shape and less than 10µm in size (265497, Sigma-Aldrich).  
10 The SEM images of the three types of particles are presented in **Figure S1**. The polymer binder  
11 solution is produced by adding 2g polylactic acid (PLA, 4032D, Natureworks LLC) to 8g  
12 dichloromethane (DCM, Sigma-Aldrich) and left to dissolve for 24 h to ensure homogenization.  
13 The steel, copper and alumina inks are prepared by mixing the corresponding particles with the  
14 polymer solution at a weight ratio of 3:1, 3:1, and 1.2:1, respectively, using a ball mill mixer  
15 (8000M Mixer/Mill, SPEX SamplePrep) for 15 min.

16

17 *Multi-material DIW:* The CAD model of the building structure is either designed in a computer  
18 aided design software (CATIA) or downloaded from internet (thingiverse.com). The support  
19 is generated where it is needed to hold building structure through a software, Simplify 3D  
20 (version 4.0). Both the building and support structures are converted into a G-code using  
21 Simplify 3D. Then the G-code is converted into a point-to-point program that can be read by  
22 the JR Point software to control the 3-axis positioning robot (I&J2200-4, I&J Fisnar). The ink  
23 is loaded in a syringe (3mL, Nordson EFD) attached with a smooth-flow tapered nozzle (exit  
24 inner diameter = 250µm, Nordson EFD). DIW is performed using the positioning robot and  
25 pressure dispensing systems (HP-7X, Nordson EFD). The structures are deposited on a glass  
26 slide (PN 16004-422, VWR) at room temperature. All the structures in this work are deposited

1 at a linear printing speed of 15mm/s and under an applied pressure of 0.7 - 1.2 MPa. The spacing  
2 between each layer is 80% of the nozzle inner diameter to compensate the solvent evaporation  
3 induced filament shrinkage and ensure tight bonding between the adjacent layers.

4  
5 *Post-deposition thermal treatment:* The as-printed structures are thermal treated in a laboratory  
6 electric tubular furnace (59256-P-COM, Lindberg) on a ceramic substrate. To prevent oxidation,  
7 a gas flow (97.5% Ar and 2.5% H<sub>2</sub>, flow rate = 5 L/min) is circulated inside the quartz tube.  
8 The temperature profile is presented in **Figure 1b**, wherein all the heating rates are 600°C/h  
9 and the cooling rate is 900°C/h.

10  
11 *Surface roughness measurement:* The roughness of the top surface of the sintered steel  
12 structures is measured using a profilometer (SV-C4000, Mitutoyo) following the AISI standard  
13 in accordance with ASME B.46.1-2002. The measuring direction is perpendicular to the  
14 filament orientation. The sampling length of meso  $R_a$  is 7.5mm, while the sampling length of  
15 micro  $R_a$  is 0.1mm. Ten specimens are measured for each sample type.

16  
17 *Porosity analysis:* The sintered steel scaffold is cut parallel to the Z direction to observe the  
18 vertical cross section. The sliced steel scaffold is sealed in a resin (EpoFix resin, Struers) block  
19 and the cross section is polished for observation under an optical microscope (Zeiss Axioplan  
20 EL-Einsatz). The porosity is determined using an image analysis software (ImageJ). The  
21 filament porosity is calculated as the ratio of void area inside the filament over the filament  
22 area. Ten cross sections of each sample are analyzed.

23  
24 *Electrical conductivity analysis:* The electrical conductivity of the sintered steel structures is  
25 measured using the four-point probes method. A constant current of 1A is provided by a power

1 supply (Agilent, E3633A). The voltage is acquired by a multimeter (HP, 3457A). Five  
2 specimens of each sample type are tested.

3

4 *Tensile test and DIC:* The samples are sintered steel tensile bars, of which the cross-section of  
5 the neck is  $\sim 3.6 \times 1.8$  mm. The tensile tests are carried out in a MTS Insight machine with a 50  
6 kN load cell (MTS 569332-01) at a crosshead speed of 1 mm/min and using DIC to measure  
7 the strain of the tensile bars. The tensile bars are polished on both sides for a smooth surface.  
8 A thin layer of white acrylic spray paint (Ultra 2X spray paint, Painter's Touch) is applied on  
9 the surface. The speckle pattern (black dots of  $\sim 0.4$ mm) is painted on the white paint with a  
10 roller brush to ensure the tracking of displacement. The images of the sample are taken by two  
11 long range focus stereo microscopes at a frequency of 4Hz during the tensile test. The images  
12 are analyzed by VIC3D micro (Correlated solutions, version 7.2.4) and the strain is calculated  
13 by the displacement of the speckle pattern. Tensile tests were performed on the sintered S, S-  
14 Cu and S-Al<sub>2</sub>O<sub>3</sub> samples and their DIC measured strains are presented in **Video S1, S2 and S3**,  
15 respectively. Five specimens for each sample type are tested.

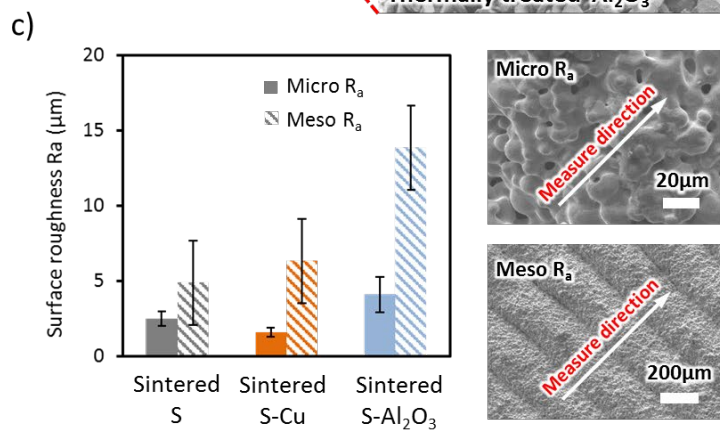
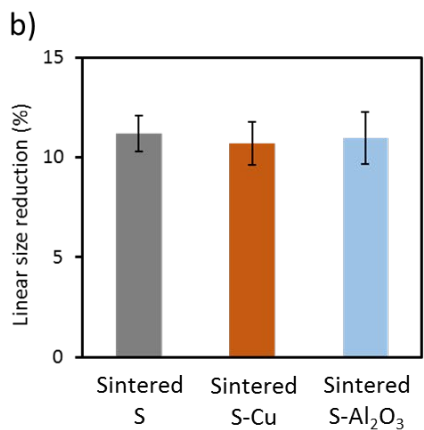
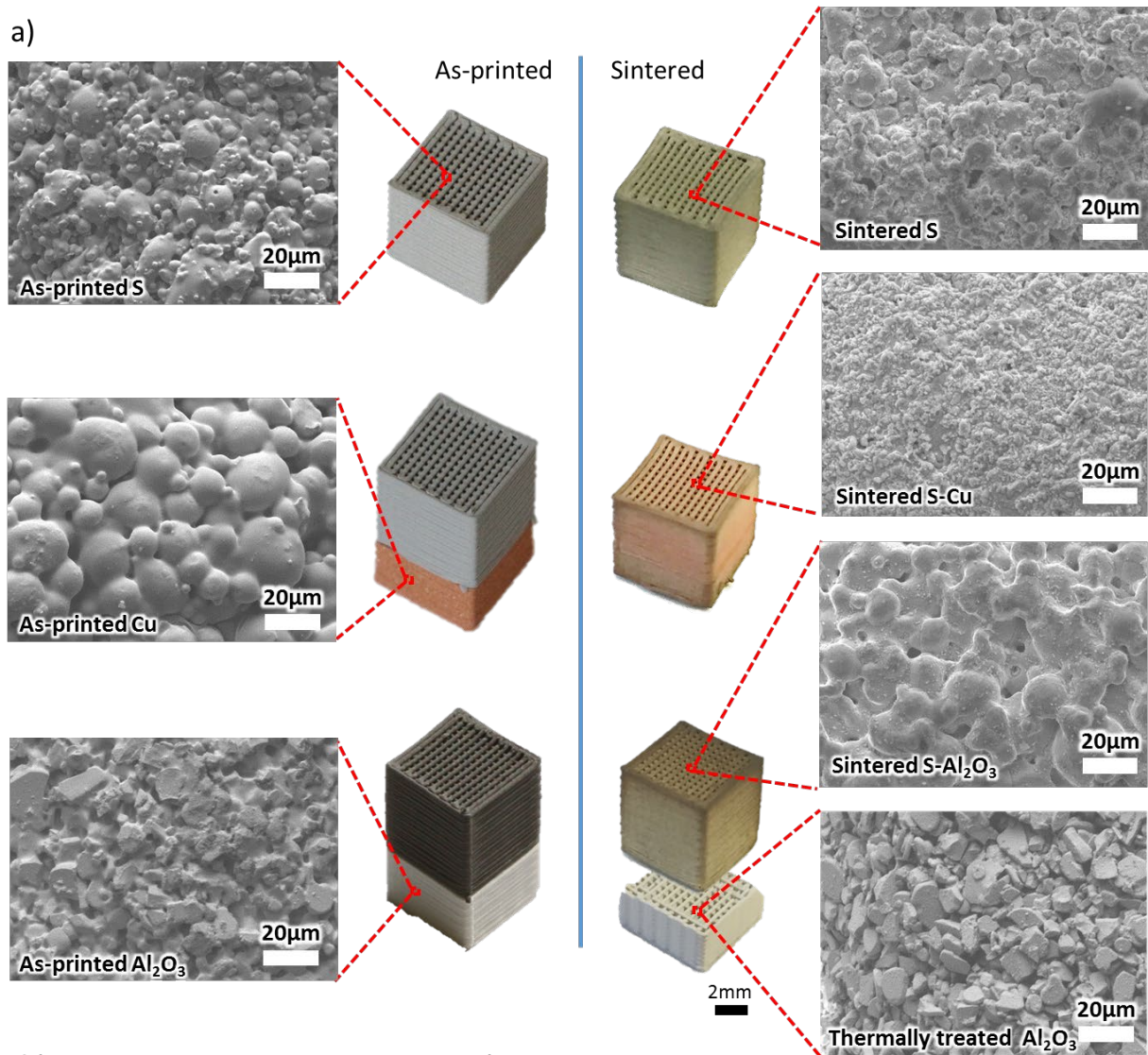
16

## 17 **Results and discussion**

18 Steel scaffolds (S), steel scaffolds with copper support (S-Cu) and steel scaffolds with alumina  
19 support (S-Al<sub>2</sub>O<sub>3</sub>) are printed and thermally treated to investigate the influence of the support  
20 materials to the building structures. **Figure 2a** shows optical and SEM images of as-printed and  
21 sintered (thermally treated) S, S-Cu and S-Al<sub>2</sub>O<sub>3</sub> scaffolds. The as-printed steel scaffolds  
22 supported by copper and alumina are as neat and orderly structured as the as-printed steel  
23 scaffold without support. The steel, copper and alumina particles are bound by the PLA binder  
24 to hold the structures, respectively. After the thermal treatment, the steel scaffolds retain their  
25 geometry, but exhibit some dimensional shrinkage. The SEM images of the sintered (thermally  
26 treated) scaffolds at different magnifications are presented in **Figure S3**. They have similar

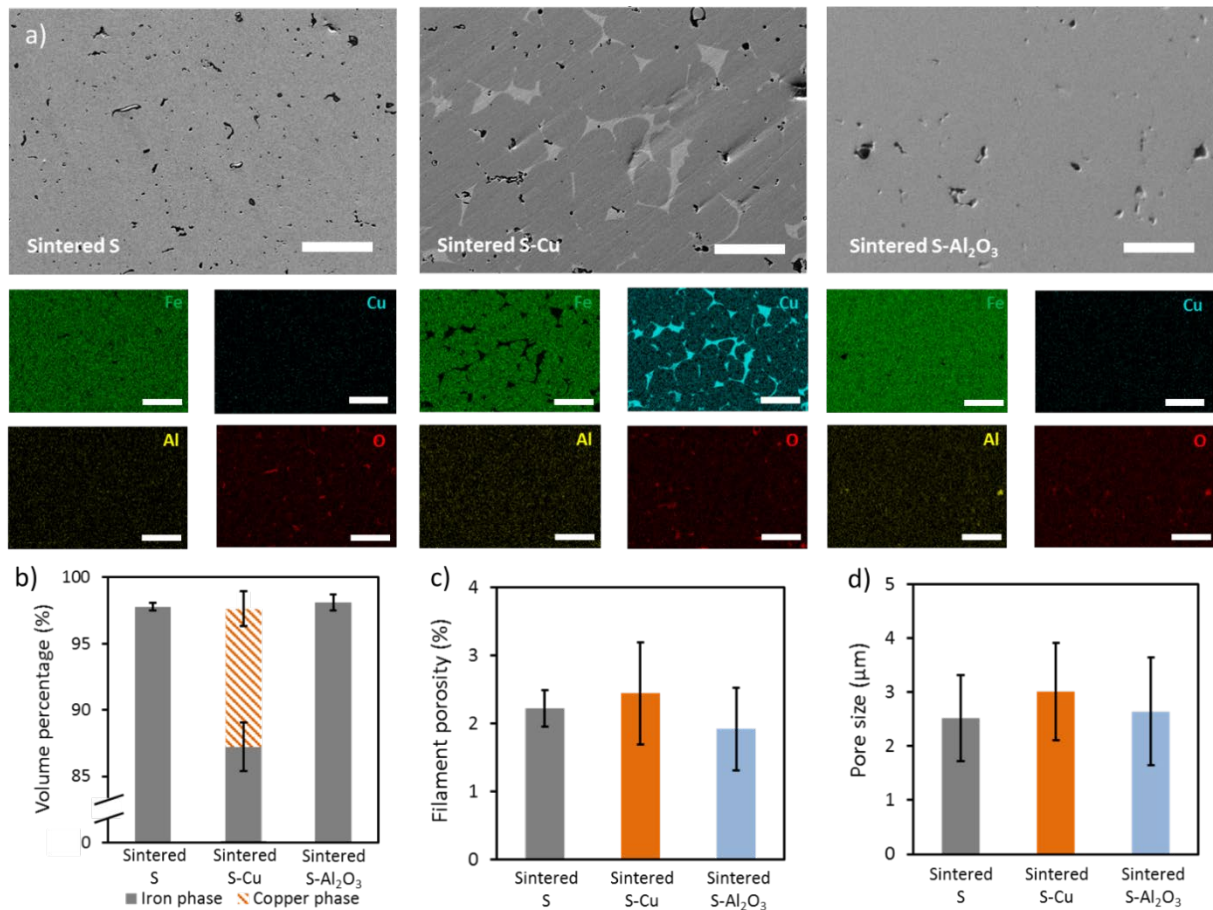
1 linear size reduction ranging from 10.7% to 11.2% (**Figure 2b**). Each type of steel scaffolds  
2 has a small size deviation of  $\leq 1.3\%$  (**Figure 2b**). The small deviation guarantees the  
3 reproducibility of this method in terms of dimensional accuracy of the fabricated structures.  
4 The steel particles of the S-Al<sub>2</sub>O<sub>3</sub> scaffold are just as sintered as those in the S scaffold, but the  
5 S-Al<sub>2</sub>O<sub>3</sub> scaffold has a rougher surface. The steel particles in S-Cu scaffold are sintered as well.  
6 In addition, the copper support melts and infiltrates into the sintered steel structure, leading to  
7 a smoother surface.

8 **Figure 2c** shows the single filament surface roughness (named as micro  $R_a$ ) and the inter-  
9 filament surface roughness (termed as meso  $R_a$ ) of the sintered steel scaffolds, and SEM images  
10 of the measured surfaces serving as an example of the micro and meso  $R_a$ . The profilometer  
11 probe traveling direction (measuring direction) is perpendicular to the filament longitudinal  
12 axis. The micro  $R_a$  of sintered S-Al<sub>2</sub>O<sub>3</sub> (4.1 $\mu\text{m}$ ) is greater than that of sintered S (2.5 $\mu\text{m}$ ), while  
13 the micro  $R_a$  of sintered S-Cu (1.6 $\mu\text{m}$ ) is smaller than that of sintered S. The meso  $R_a$ s of  
14 sintered S and sintered S-Cu are similar ( $\sim 5\mu\text{m}$ ), which are smaller than that of sintered S-Al<sub>2</sub>O<sub>3</sub>  
15 (13.9 $\mu\text{m}$ ). The thermally treated alumina scaffold is so fragile that the shrinkage and surface  
16 roughness could not be measured. The shrinkage difference between the thermally treated  
17 ceramic particles and the sintered steel particles leads to a rougher surface. According to our  
18 observations, the support materials have little influence on the dimensional shrinkage of the  
19 steel scaffolds. The alumina support appears to increase the micro and meso surface roughness  
20 of the sintered steel structure by 1.6 $\mu\text{m}$  and 9 $\mu\text{m}$ , respectively.



1  
2 **Figure 2.** (a) Optical and SEM images of as-printed and sintered (thermal treated) scaffolds.  
3 (b) Linear size reduction of the sintered steel structures. (c) Single filament surface roughness  
4 (micro  $R_a$ ) and inter-filament surface roughness (meso  $R_a$ ) of the sintered steel structures, and  
5 SEM images of the measured surfaces serving as an example of the micro and meso  $R_a$ .

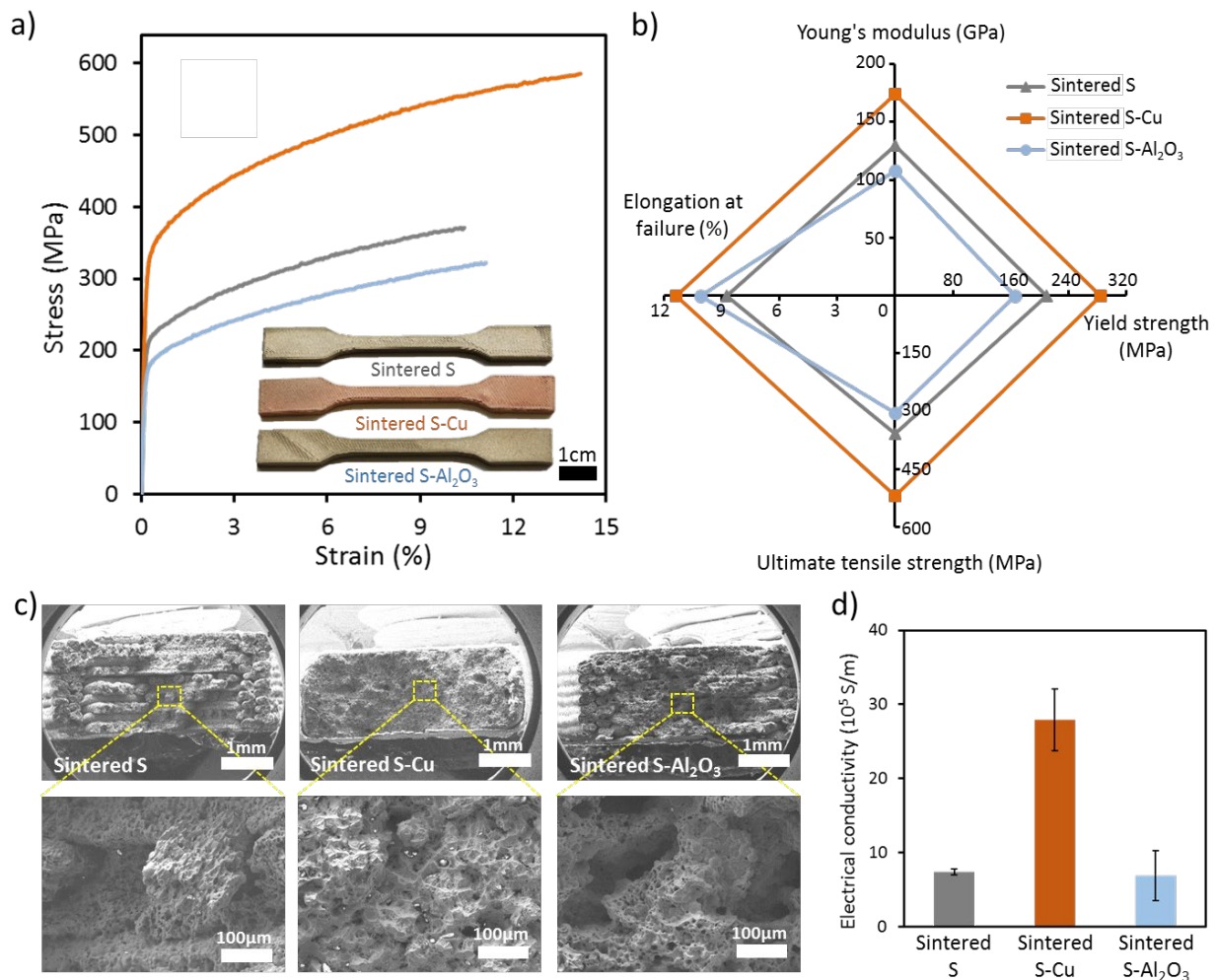
1 The influence of the support materials to the elemental composition and porosity of the building  
2 structures is studied through SEM and elemental analysis. **Figure 3a** shows SEM images and  
3 Energy-dispersive X-ray spectroscopy (EDS) elemental mappings of the cross sections of  
4 sintered S, sintered S-Cu, and sintered S-Al<sub>2</sub>O<sub>3</sub> structures. The cross sections of the three types  
5 of sintered steel structures are characterized by the strong presence of iron. Copper is detected  
6 only in the sintered S-Cu structures as expected. The detection of copper is located in the regions  
7 between the iron rich zones. Aluminum and oxygen (i.e., the elements contained in the alumina  
8 support) are not detected in the sintered S-Al<sub>2</sub>O<sub>3</sub> structures. Neither in the sintered S and  
9 sintered S-Cu structures. The elemental analysis result shows that: (i) the copper support  
10 infiltrates into the building structure and fills the majority of the pores in the sintered steel  
11 structure during the thermal treatment, and (ii) the alumina support is chemically stable during  
12 the thermal treatment and does not contaminate the steel structure. The volume fractions of the  
13 solid phases (iron for S and S-Al<sub>2</sub>O<sub>3</sub>, iron and copper for S-Cu) are similar in all three types of  
14 sintered steel structures at ~ 98% (**Figure 3b**). In the sintered S-Cu structure, the iron phase  
15 takes up about 87.2% and the copper phase accounts for around 10.4%. This value can be  
16 controlled by the volume ratio of the support and building structure, which will be studied in  
17 the future work. All the three types of sintered steel structures have similar and low porosity  
18 (~2%), and small pore size between 2 and 3 μm (Figure 3c-d). The supports do not have an  
19 obvious influence on the porosity and pore size to the building structure.



1  
2 **Figure 3.** Elemental and porosity analysis of the sintered steel structures. (a) SEM images and  
3 EDS elemental mappings of the cross sections of sintered S, sintered S-Cu, and sintered S-  
4 Al<sub>2</sub>O<sub>3</sub> structures. Scale bar = 50μm. (b) Volume percentage of iron and copper phase, (c)  
5 filament porosity, and (d) filament pore size of the various sintered steel structures.

6  
7 Figure 4 shows the results for the electrical and tensile tests conducted on the sintered steel  
8 structures manufactured using different support materials.. **Figure 4a** presents typical tensile  
9 stress-strain curves and representative optical image of the sintered S, S-Cu and S-Al<sub>2</sub>O<sub>3</sub> tensile  
10 bars in the inset. **Figure S4** presents the SEM images of the sintered S, S-Cu and S-Al<sub>2</sub>O<sub>3</sub> fully  
11 dense tensile bars. Stereoscopic digital image correlation (DIC) technique is used to measure  
12 the strain in the tensile bars during the tensile tests (**Figure S5**). The measured tensile properties  
13 of the sintered steel structures are shown in **Figure 4b**. Sintered S-Cu exhibits higher Young's  
14 modulus  $E$  ( $174 \pm 10$  GPa), yield strength ( $YS$ ) ( $284 \pm 16$  MPa) and ultimate tensile strength

1 (*UTS*) ( $521 \pm 57$  MPa) and elongation at failure ( $11.3\% \pm 3.6\%$ ) compared to those of sintered  
2 S ( $\sim 30\%$  -  $45\%$  superior). This increase in tensile properties is the result of copper infiltration  
3 of the sintered steel structure. Sintered S-Al<sub>2</sub>O<sub>3</sub> has weaker tensile properties compared to the  
4 sintered S. The *E* ( $108 \pm 6$  GPa), the *YS* ( $165 \pm 8$  MPa) and the *UTS* ( $304 \pm 18$  MPa) of sintered  
5 S-Al<sub>2</sub>O<sub>3</sub> are  $15\%$  -  $21\%$  less than those of sintered S. The elongation at failure ( $10.1\% \pm 1.4\%$ )  
6 of sintered S-Al<sub>2</sub>O<sub>3</sub> is similar to that of sintered S. We believe that the dimensional shrinkage  
7 difference between the steel structure and the alumina support might affect the sintering of the  
8 steel structure and lead to weaker tensile properties. **Figure 4c** shows the SEM images of the  
9 tensile fracture surfaces of the sintered steel tensile bars. More SEM images of the tensile  
10 fracture surfaces at different magnification are presented in **Figure S6**. The tensile fracture  
11 surface of the sintered S shows the shape and orientation of individual filaments at  $45^\circ$  relative  
12 to the tensile direction and orthogonal with the filaments from adjacent layers. Each individual  
13 filament is dense and the filaments from the same and the neighboring layers are fused together.  
14 The individual filament shape and orientation are recognizable but not very clear in the sintered  
15 S-Al<sub>2</sub>O<sub>3</sub>. The filaments in sintered S-Cu are completely fused together with the presence of  
16 copper, making a fully dense structure. The electrical conductivity of the sintered S-Al<sub>2</sub>O<sub>3</sub> is  
17  $(6.9 \pm 3.4) \times 10^5$  S/m and the sintered S,  $(7.4 \pm 0.4) \times 10^5$  S/m are similar (**Figure 4d**). The  
18 electrical conductivity of sintered S-Cu,  $(27.9 \pm 4.2) \times 10^5$  S/m, is approximately four times  
19 higher than the value measure for the sintered S due to the presence of copper (**Figure 4d**). The  
20 properties of the sintered steel structures are summarized in **Table S1**. The overall electrical  
21 and mechanical properties of the sintered S-Cu are superior to those of the sintered S. Sintered  
22 S-Al<sub>2</sub>O<sub>3</sub> has comparable electrical properties, but slightly weaker mechanical properties  
23 compared to the sintered S.



1  
2 **Figure 4.** Electrical and mechanical characterizations of the sintered steel structures. (a) Typical  
3 tensile stress-strain curves of sintered steel structures and representative optical image of the  
4 different sintered steel tensile bars (inset). (b) Young's modulus, yield strength, ultimate tensile  
5 strength and elongation at failure of the sintered steel structures. (c) SEM images of the tensile  
6 fracture surfaces of the sintered steel structures. (d) Electrical conductivity of the sintered steel  
7 structures.

8  
9 **Conclusion**

10 A multi-material direct ink writing method is developed to fabricate complex 3D metallic  
11 structures by printing removable supports using two different secondary materials. As a proof  
12 of concept, steel structures are fabricated through this method with the help of copper and  
13 alumina supports, respectively. The influence of the support materials on the steel structure is

1 investigated. The supports lead to no significant difference to the building structures on the  
2 dimensional shrinkage, surface roughness and porosity of the building structure. The copper  
3 support brings a hybrid metallic composition to the steel structure and improves its electrical  
4 conductivity by four times and stiffness by 34%. Although the alumina supports lower the  
5 stiffness of the building structure by 17%, it brings no contamination to the steel structure. It is  
6 worth mentioning that the support materials are not only limited to copper or alumina. Any  
7 desired alloying metal with a lower melting point than the building material can be the metal  
8 support material, e.g., zinc and aluminum. Any ceramic material that is physically and  
9 chemically stable during the thermal treatment can be the ceramic support materials such as  
10 tungsten carbide. The proposed method broadens the geometry possibilities of metallic 3D  
11 structures that DIW can create. It provides the metal additive manufacturing of medical  
12 implants, sensors and batteries featuring complex geometries a readily accessible choice.

13

#### 14 **Supporting Information**

15 SEM images, the strain distribution measured by DIC, a summary of the properties of the  
16 sintered steel structures, videos of the tensile test process with DIC measured strain showing  
17 on the samples.

18

#### 19 **Author Contributions**

20 The manuscript was written through contributions of all authors. All authors have given  
21 approval to the final version of the manuscript.

22

#### 23 **Corresponding Author**

24 (Daniel Therriault) Email: [daniel.therriault@polymtl.ca](mailto:daniel.therriault@polymtl.ca)

25

1 **Conflict of Interest**

2 The authors declare no conflict of interest.

3

4 **Acknowledgements**

5 The authors acknowledge the financial support from NSERC (Natural Sciences and  
6 Engineering Research Council of Canada, grant number: RGPIN 312568-2013) and Auto 21 of  
7 the Canadian Network of Centers of Excellence (NCE) program. The authors also acknowledge  
8 the scientific discussions from Olivier Sioui-Latulippe and Vincent Wuelfrath-Poirier on  
9 metallurgy science. A scholarship for Mr. Xu was also provided by the China scholarship  
10 Council (CSC) and the Fonds de recherche du Quebec - Nature et technologies (FRQNT).

11

1   References

- 2       1. Cheng, M., Jiang, Y., Yao, W., Yuan, Y., Deivanayagam, R., Foroozan, T., Huang, Z.,  
3       Song, B., Rojaee, R., Shokuhfar, T., Pan, Y., Lu, J., Shahbazian-Yassar, R. Elevated-  
4       Temperature 3D Printing of Hybrid Solid-State Electrolyte for Li-Ion Batteries. *Adv.*  
5       *Mater.* **2018**, 30, 1800615.
- 6       2. Finsterbusch, M., Danner, T., Tsai, C.L., Uhlenbruck, S., Latz, A., Guillon, O. High  
7       Capacity Garnet-Based All-Solid-State Lithium Batteries: Fabrication and 3D-  
8       Microstructure Resolved Modeling. *ACS Appl. Mater. Interfaces* **2018**, 10, 22329–  
9       22339.
- 10      3. Elahinia, M., Moghaddam, N.S., Andani, M.T., Amerinatanzi, A., Bimber, B.A.,  
11      Hamilton, R.F. Fabrication of NiTi through Additive Manufacturing: A Review. *Prog.*  
12      *Mater. Sci.* **2016**, 83, 630-663.
- 13      4. Amin Yavari, S., Loozen, L., Paganelli, F.L., Bakhshandeh, S., Lietaert, K., Groot, J.A.,  
14      Fluit, A.C., Boel, C.H.E., Alblas, J., Vogely, H.C., Weinans, H. Antibacterial Behavior  
15      of Additively Manufactured Porous Titanium with Nanotubular Surfaces Releasing  
16      Silver Ions. *ACS Appl. Mater. Interfaces* **2016**, 8, 17080-17089.
- 17      5. Rim, Y.S., Bae, S.H., Chen, H., De Marco, N., Yang, Y. Recent Progress in Materials  
18      and Devices toward Printable and Flexible Sensors. *Adv. Mater.* **2016**, 28, 4415-4440.
- 19      6. Xu, L., Gutbrod, S.R., Bonifas, A.P., Su, Y., Sulkin, M.S., Lu, N., Chung, H.J., Jang,  
20      K.I., Liu, Z., Ying, M., Lu, C., Webb, R. C., Kim, J. S., Laughner, J. I., Cheng, H., Liu,  
21      Y., Ameen, A., Jeong, J. W., Kim, G. T., Huang, Y., Efimov, I. R., Rogers, J. A. 3D  
22      Multifunctional Integumentary Membranes for Spatiotemporal Cardiac Measurements  
23      and Stimulation across the Entire Epicardium. *Nat. Commun.* **2014**, 5, 4329.
- 24      7. Gu, D.D., Meiners, W., Wissenbach, K. Poprawe, R. Laser Additive Manufacturing of  
25      Metallic Components: Materials, Processes and Mechanisms. *Int. Mater. Rev.* **2012**,  
26      57, 133-164.

- 1 8. Herzog, D., Seyda, V., Wycisk, E., Emmelmann, C. Additive Manufacturing of Metals.  
2 *Acta Mater.* **2016**, 117, 371-392.
- 3 9. Martin, J.H., Yahata, B.D., Hundley, J.M., Mayer, J.A., Schaedler, T.A., Pollock, T.M.  
4 3D Printing of High-strength Aluminium Alloys. *Nature* **2017**, 549, 365.
- 5 10. Gong, H., Rafi, K., Gu, H., Ram, G.J., Starr, T., Stucker, B. Influence of Defects on  
6 Mechanical Properties of Ti-6Al-4 V Components Produced by Selective Laser  
7 Melting and Electron Beam Melting. *Mater. Des.* **2015**, 86, 545-554.
- 8 11. Olakanmi, E.O.T., Cochrane, R.F., Dalgarno, K.W. A Review on Selective Laser  
9 Sintering/Melting (SLS/SLM) of Aluminium Alloy Powders: Processing,  
10 Microstructure, and Properties. *Prog. Mater. Sci.* **2015**, 74, 401-477.
- 11 12. Chou, R., Milligan, J., Paliwal, M., Brochu, M. Additive manufacturing of Al-12Si  
12 Alloy via Pulsed Selective Laser Melting. *JOM* **2015**, 67, 590-596.
- 13 13. Skylar-Scott, M.A., Gunasekaran, S. and Lewis, J.A., Laser-assisted Direct Ink Writing  
14 of Planar and 3D Metal Architectures. *Proc. Natl. Acad. Sci. U. S. A.* **2016**, 113, 6137-  
15 6142.
- 16 14. Wang, X., Guo, Q., Cai, X., Zhou, S., Kobe, B. and Yang, J., Initiator-integrated 3D  
17 Printing Enables the Formation of Complex Metallic Architectures. *ACS Appl. Mater.*  
18 *Interfaces* **2013**, 6, 2583-2587.
- 19 15. Lewis, J. A. Direct Ink Writing of 3D Functional Materials. *Adv. Funct. Mater.* **2006**,  
20 16, 2193-2204.
- 21 16. Therriault, D., White, S.R., Lewis, J.A. Chaotic Mixing in Three-dimensional  
22 Microvascular Networks Fabricated by Direct-write Assembly. *Nat. Mater.* **2003**, 2, 265.
- 23 17. Ahn, B.Y., Shoji, D., Hansen, C.J., Hong, E., Dunand, D.C., Lewis, J.A. Printed  
24 Origami Structures. *Adv. Mater.* **2010**, 22, 2251-2254.

- 1 18. Jakus, A.E., Taylor, S.L., Geisendorfer, N.R., Dunand, D.C., Shah, R.N. Metallic  
2 Architectures from 3D-printed Powder-based Liquid Inks. *Adv. Funct. Mater.* **2015**, 25,  
3 6985-6995.
- 4 19. Xu, C., Bouchemit, A., L'Espérance, G., Lebel, L.L., Therriault, D. Solvent-cast based  
5 Metal 3D Printing and Secondary Metallic Infiltration. *J. Mater. Chem. C* **2017**, 5,  
6 10448-10455.
- 7 20. Xu, C., Wu, Q., L'Espérance, G., Lebel, L.L., Therriault, D. Environment-friendly and  
8 Reusable Ink for 3D Printing of Metallic Structures. *Mater. Des.* **2018**, 160, 262-269.
- 9 21. Ziemian, C.W., Crawn III, P.M. Computer Aided Decision Support for Fused  
10 Deposition Modeling. *Rapid Prototyp J* **2001**, 7, 138-147.
- 11 22. Waheed, S., Cabot, J.M., Macdonald, N.P., Lewis, T., Guijt, R.M., Paull, B., Breadmore,  
12 M.C. 3D Printed Microfluidic Devices: Enablers and Barriers. *Lab Chip* **2016**, 16, 1993-  
13 2013.
- 14 23. Peckner, D., Bernstein, I. M. *Handbook of Stainless Steels*; McGraw-Hill Book  
15 Company, New York, 1997.
- 16 24. Davis, J. R. *Copper and Copper Alloys*; ASM international, 2001.
- 17 25. Pradyot, P. *Handbook of Inorganic Chemicals*; McGraw-Hill, New York, 2003.
- 18

# Table of Contents

A multi-material direct ink writing (DIW) method is developed to fabricate complex three-dimensional (3D) steel structures by creating a removable support printed from a lower melting temperature metal (i.e., copper) or a ceramic (i.e., alumina). The lower melting temperature metal completely infiltrates the porous steel structures for a hybrid configuration, while the ceramic offers a brittle support that can be easily removed.

**Keyword:** additive manufacturing, direct ink writing, complex 3D metallic structures, removable support, multi-material

**Authors:** Chao Xu, Bronagh Quinn, Gilles L'Espérance, Louis Laberge Lebel, Daniel Therriault\*

**Title:** Multi-material direct ink writing (DIW) for complex 3D metallic structures with removable supports

